Since January 2020 Elsevier has created a COVID-19 resource centre with free information in English and Mandarin on the novel coronavirus COVID-19. The COVID-19 resource centre is hosted on Elsevier Connect, the company's public news and information website.

Talanta 226 (2021) 122160

Contents lists available at ScienceDirect

Talanta

journal homepage: www.elsevier.com/locate/talanta

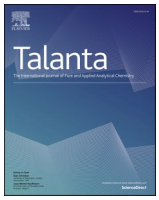

Preparation of IgG imprinted polymers by metal-free visible-light-induced ATRP and its application in biosensor

Ru Bai, Yue Sun *, Mengyuan Zhao, Zhen Han, Juntong Zhang, Yuze Sun, Wenjing Dong, Siyu Li

School of Chemistry and Chemical Engineering, Liaoning Normal University, Dalian, 116029, China

ARTICLE INFO

Keywords:
Metal-free visible-light-induced ATRP
Molecular imprinted polymers
Immunoglobulin G
Electrochemical biosensor

ABSTRACT

Immunoglobulin G (IgG) is related to the occurrence of many diseases, such as measles and inflammatory. In this paper, IgG imprinted polymers (IgGIPs) were fabricated on the surface of nano Au/nano Ni modified Au electrode (IgGIPs/AuNCs/NiNCs/Au) via metal-free visible-light-induced atom transfer radical polymerization (MVL ATRP). The IgGIPs were prepared by IgG conjugated with fluorescein isothiocyanate (FITC-IgG) as both a template and a photocatalyst. After the templates were removed, the photocatalysts (FITC) would not remain in the polymer and avoided all the effect of catalysts on the electrode. The fabricated electrodes were examined by cyclic voltammetry (CV), electrochemical impedance spectroscopy (EIS), scanning electron microscope (SEM) and X-ray photoelectron spectroscopy (XPS). Under the optimized conditions, IgGIPs/AuNCs/NiNCs/Au was prepared and used as an electrochemical biosensor. The biosensor could be successfully applied for the determination of IgG by differential pulse voltammetry (DPV) measurement. The results showed that the proposed biosensor displayed a broader linear range and a lower detection limit for IgG determination when it was compared to those similar IgG sensors. The linear range from 1.0×10^{-6} mg L^{-1} to 1.0×10^{1} mg L^{-1} was obtained with a low detection limit (LOD) of 2.0×10^{-8} mg L^{-1} ($S/N = 3$). Briefly, the biosensor in this study introduced an easy and non-toxic method for IgG determination and also provided a progressive approach for designing protein imprinted polymers.

1. Introduction

Immunoglobulin G (IgG) is the most important antibody for the mammal with antiviral, neutralizing virus, antibacterial and immunomodulatory functions, and it is always closely related to the occurrence of many diseases, such as measles, inflammatory, primary and secondary immuno-deficiencies [1–9]. At present, the detection of IgG antibody in blood is also one of the crucial methods to determine the infection of COVID-19 [10]. Accurate determination of trace IgG plays an essential role in clinical detection as well as in basic medical research. Common ways for IgG detection are enzyme-linked immunosorbent assay (ELISA) [11], fluoroimunoassays [12], electrochemical immunosensor [3] and chemiluminescence immunoassays [13]. However, these methods usually need antibody, which is difficult to prepare, purify and preserve. These drawbacks prompt researchers to explore better stability and low-cost methods for IgG detection.

Molecular imprinted polymers are generally considered to be substituents of natural antibodies [14–17], which are synthesized by forming a polymer network around the template. When the template is removed, chemically and spatially complementary voids (imprints) are left in the polymer network that are capable of recombining the template [18]. To date, the imprinting technique of small molecules has been well-established [19–21], while there are still some difficulties for the successful imprinting of proteins. The large molecular weight and the slow mass transfer rate of the protein result in the bad recognition of imprinted polymers. Aiming at overcoming these problems, scientists have proposed surface imprinting, that is, limit all binding sites to the accessible surfaces for removal and binding of proteins [22]. Normally, surface imprinting needs a thin polymer layer on the surface of the carrier, thus it puts forward higher request to the preparation technology of polymers.

"Living"/controlled atom transfer radical polymerization (ATRP) is one of the most efficient techniques for synthesis of polymers with tunable molecular weights, low dispersities, defined chemical composition and complex architecture [23–25], and is also an important technique for designing and preparing protein imprinted polymers. For example, *Yildirim* et al. [26] designed myoglobin imprinted polymer films on silicon wafers by surface-initiated ATRP. *Naraprawatphong* et al.

* Corresponding author.
E-mail address: yuesun@lnnu.edu.cn (Y. Sun).

https://doi.org/10.1016/j.talanta.2021.122160
Received 17 July 2020; Received in revised form 22 January 2021; Accepted 26 January 2021
Available online 29 January 2021

[27] successfully synthesized IgG-recognition SPR devices by combination of surface-initiated ATRP with imprinted polymers. *Gai* et al. [28] developed a bovine serum albumin imprinted magnetic polymer based on ATRP method for protein separation. However, the traditional ATRP has two drawbacks. First, the catalyst of low-cost transition metal is sensitive to air, leading to the anaerobic polymerization. Second, the residual catalyst has certain toxicity to the protein [25,29]. Therefore, improved ATRP needs to be explored for better use in the preparation of protein imprinted polymers.

Metal-free visible-light-induced ATRP (MVL ATRP) was conducted by using photocatalysts instead of metal salts [30,31]. Typically, these photocatalyst has a high excited oxidation potential and can initiate the polymerization by dechlorinating the halide (initiator of ATRP) to provide radical species. MVL ATRP has a simple operation, fast polymerization rate, high conversion rate, mild polymerization condition, more importantly, it can obtain both well-defined polymers and no metal pollution [29,32,33]. Fluorescein is a photocatalyst commonly used in MVL ATRP, which has visible light absorption, good chemical stability, long excited state lifetime and good redox potential [34,35]. However, Fluorescein is usually colored and also remained in the imprinted polymers, which will affect the subsequent analysis of imprinted polymers.

In order to retain the advantages of MVL ATRP and eliminate all effects of catalysts, in this paper, IgG imprinted polymers (IgGIPs) were prepared by IgG conjugated with fluorescein isothiocyanate (FITC-IgG) as both a template and a photocatalyst. After the templates were removed, the photocatalyst would not remain. The IgGIPs were prepared on the surface of Au electrode which had been modified with nano Au/nano Ni (IgGIPs/AuNCs/NiNCs/Au) to enhance the area and promote the electron transfer ability of the electrode [36]. The obtained IgGIPs/AuNCs/NiNCs/Au electrode can be used as a biosensor for the detection of IgG. Compared with the similar sensors, the IgGIPs/AuNCs/NiNCs/Au prepared by MVL ATRP had better recognition and would have wider application in the field of biosensor fabrication.

2. Materials and methods

2.1. Chemicals

Au electrode ($\Phi = 2$ mm) was purchased from Chenhua Instruments Co. (Shanghai, China). Acrylamide (AM, functional monomer), N, N′-methylene bis-acrylamide (MBA, cross-linker), ammonium persulfate, triethylamine (TEA), nickel sulfate, boric acid, ammonium chloride and sodium dodecylsulfate (SDS) were obtained from Kemiou Chemical Co. (Tianjin, China). Chloroauric acid ($HAuCl_4{\cdot}4H_2O$) was purchased from Beijing chemical plant (Beijing, China). Mouse immunoglobulin G (IgG, MW 150 kDa), Human immunoglobulin M (IgM, MW 970 kDa), Human immunoglobulin A (IgA, MW 400 kDa), FITC-IgG, myoglobin (Mb, MW 16.7 kDa), human serum albumin (HSA, MW 69 kDa) and bovine hemoglobin (Hb, MW 65 kDa) were supplied by Solarbio Inc. (Beijing, China). Nickel chloride and saccharin were supplied from Aladdin Industrial Co. (Shanghai, China). Phosphate buffered solution (PBS) was prepared using 0.1 mol/L Na_2HPO_4 and 0.1 mol/L KH_2PO_4. All the chemicals were analytical reagent (AR) grade and used without any further purification. All the water used in the experiments was the hyperpure water (resistivity > 18 MΩ cm).

2.2. Apparatus

Light-emitting diode lamp was used as visible light and purchased from Duration Power Technology Co., Ltd. (Guangzhou, China). Electrochemical measurements were carried out on a CHI660D electrochemical workstation (Chenhua, Shanghai, China) with a three-electrode system, which was configured by connecting a bare or modified Au electrode, a Pt wire, and a saturated calomel electrode (SCE) as a working electrode, counter electrode, and reference electrode, respectively. The CV characterization was carried out at a scanning rate of 0.1 V/s with a potential range from −0.2 to 0.6 V. EIS was accomplished within the frequency range of 5 mHz–10 kHz. The morphologies of polymers/AuNCs/NiNCs/Au and IgGIPs/AuNCs/NiNCs/Au were observed using a scanning electron microscope (SEM, SU8010, Hitachi, Japan) at an accelerating voltage of 5.0 kV. X-ray photoelectron spectroscopy (XPS) was obtained with Thermo ESCALAB 250Xi spectrometer using a monochromatic Al Kα radiation.

2.3. Preparation of IgGIPs/AuNCs/NiNCs/Au

The synthesis of IgGIPs/AuNCs/NiNCs/Au was illustrated in Fig. 1. AuNCs/NiNCs/Au was firstly prepared according to the method reported previously [36]. The as-prepared thiol initiator, which was synthesized based on literature [37], was immobilized on the surface of AuNCs/NiNCs/Au as reported early [38]. Then the monomer (AM, 1.2500 g), cross-linker (MBA, 0.8516 g), template (IgG, 0.0020 g; FITC-IgG, 4 μL) and TEA (0.25 mL) were dissolved in PBS (pH 7.4, 18.75 mL). After purging with nitrogen for 10 min, the initiator modified electrode was inserted into the solution and illuminated under visible light for 6 h to conduct the polymerization on the surface of AuNCs/-NiNCs/Au electrode.

The IgG template was removed from the electrode by soaking in 10% (v/v) CH_3COOH solution containing 10 g/L SDS for 1 h and assisted by electric potential of −0.6 V [39]. After washing with PBS three times, the AuNCs/NiNCs/Au modified with IgGIPs (IgGIPs/AuNCs/NiNCs/Au) was obtained.

The non-imprinted polymers modified electrode (NIPs/AuNCs/NiNCs/Au) was synthesized by the same method without mouse IgG and replacing FITC-IgG with fluorescein.

2.4. Determination of IgG

The determination of IgG by IgGIPs/AuNCs/NiNCs/Au electrode was studied by measuring the intensity of the peak current of a redox probe by DPV method using PBS (pH 7.0) containing 0.1 M KCl and 5 mM $[Fe(CN)_6]^{3-/4-}$ as electrolyte. For this, the DPV of $[Fe(CN)_6]^{3-/4-}$ redox probe was firstly recorded by prepared IgGIPs sensor from 0.00 to 0.45 V with an increment potential of 4 mV, amplitude of 50 mV, a pulse width of 0.2 s and a pulse period of 0.5 s. Then this sensor was incubated in IgG solution for 5 min and rinsed three times with PBS solution, it was placed in electrolyte and the corresponding DPV of $[Fe(CN)_6]^{3-/4-}$ was recorded again. Quantitative analysis of IgG was done based on the signal response (ΔI), which was the difference of the peak current of redox probe in the absence and presence of template IgG.

3. Results and discussion

3.1. Characterization of IgGIPs/AuNCs/NiNCs/Au

The surface of the modified electrode was observed by SEM and shown in Fig. 2. As could be seen, AuNCs/NiNCs/Au showed flowers structure with a diameter of about 300 nm (Fig. 2A and D). After the polymerization, polymers/AuNCs/NiNCs/Au (Fig. 2B) and IgGIPs/AuNCs/NiNCs/Au (Fig. 2C) had the similar morphology with AuNCs/NiNCs/Au (Fig. 2A) at low magnification. When they were observed at high magnification, obvious differences could be seen. A blurred edge appeared on the surface of AuNCs/NiNCs/Au electrode due to the formation of a polymer film (Fig. 2E), while a porous topology appeared on the surface of IgGIPs/AuNCs/NiNCs/Au in Fig. 2F, which could be attributed to the imprinted structures formed by the elution of IgG from polymers/AuNCs/NiNCs/Au.

CV and EIS were used to efficiently indicate the changes on the electrode surface after each modification step. Fig. 3A demonstrated the results of CV characterization. It could be clearly seen that there was an approximately reversible redox peak of $[Fe(CN)_6]^{3-/4-}$ probe at the bare

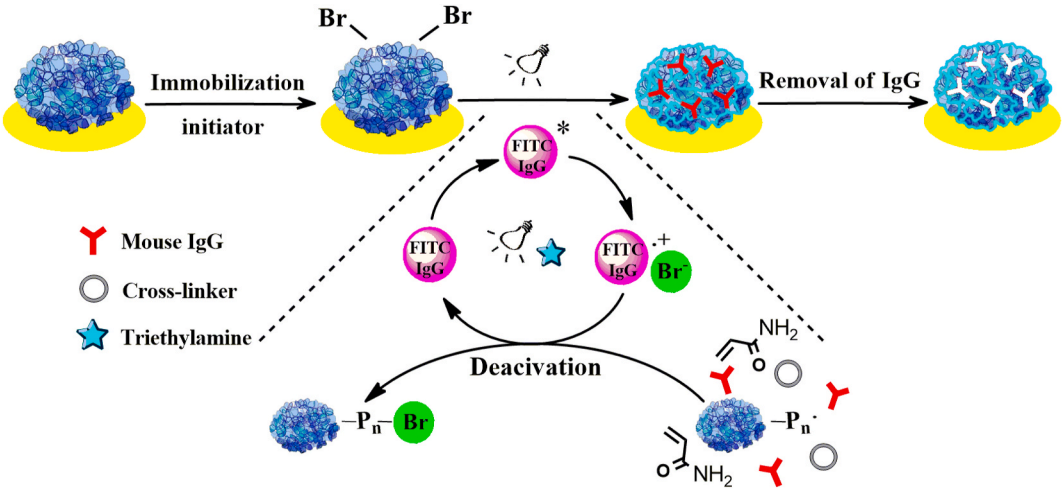

Fig. 1. Schematic preparation process of IgGIPs/AuNCs/NiNCs/Au via MVL ATRP.

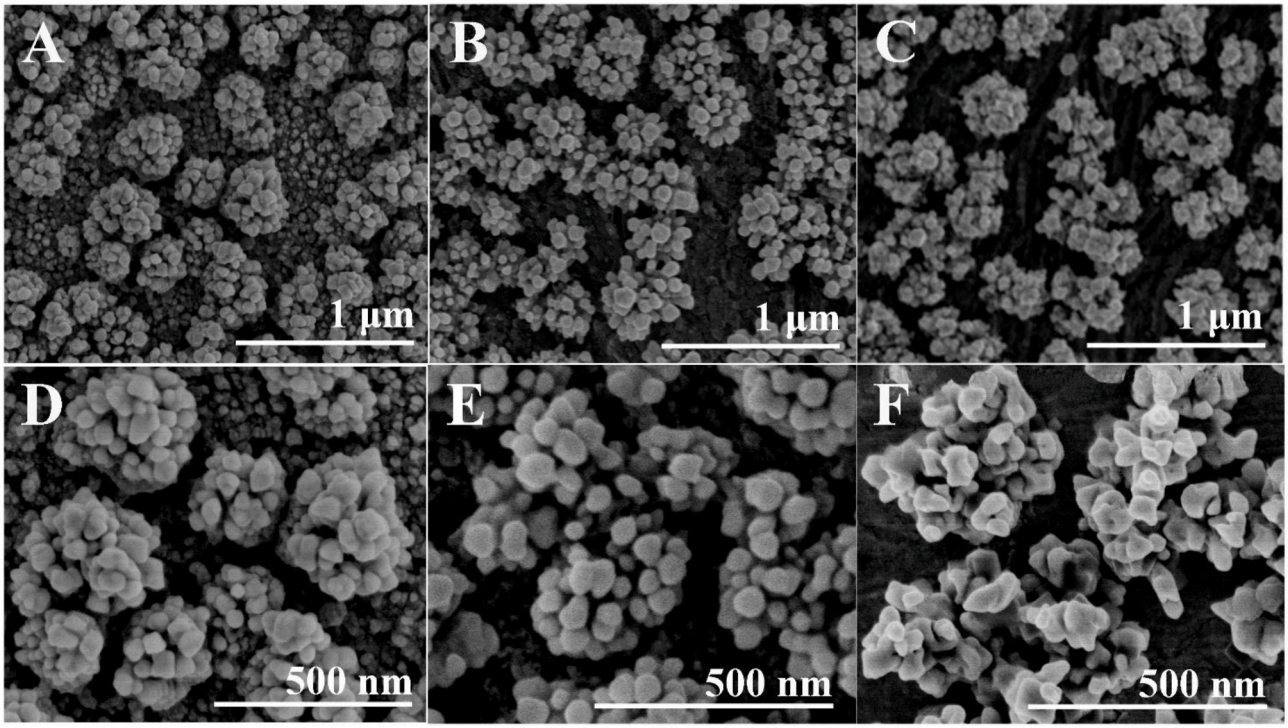

Fig. 2. SEM images of AuNCs/NiNCs/Au (A, D), polymers/AuNCs/NiNCs/Au (B, E) and IgGIPs/AuNCs/NiNCs/Au (C, F) at different magnification.

Au (Fig. 3A curve 1), showing the conducting nature of bare electrode [40]. Decoration of nano Au/nano Ni on the surface of bare gold increased evidently the peak current (Fig. 3A curve 2), indicating nanomaterials enlarged the effective electrode surface area and raised electron transfer rate [36]. For polymers/AuNCs/NiNCs/Au electrode (Fig. 3A curve 3), the diffusion of the $[Fe(CN)_6]^{3-/4-}$ probe to the electrode surface was difficult due to the high resistance and poor electron transfer ability of the compact membrane. As a result, the CV peak current decreased significantly. After removing the mouse IgG, the peak current was sharply enhanced (Fig. 3A curve 4), which may be attributed to the imprinted holes, making the $[Fe(CN)_6]^{3-/4-}$ probe easier to diffuse to the electrode surface.

Fig. 3B showed the EIS of stepwise modified electrodes, of which the results were consistent with those from CV tests. Bare Au electrode revealed a small semicircle domain (Fig. 3B curve 1), implying a low R_{et} on the bare Au electrode. It was evident that introduction of nano Au/nano Ni improved the conductivity and enlarged surface area of the electrode (Fig. 3B curve 2), resulting in the lower R_{et} [36]. By formation of polymers onto the AuNCs/NiNCs/Au surface (Fig. 3B curve 3), R_{et} became significantly larger due to the inertness of polymers. After removing the IgG (Fig. 3B curve 4), R_{et} became smaller than that of polymers/AuNCs/NiNCs/Au, suggesting that the imprinted holes appeared on IgGIPs/AuNCs/NiNCs/Au, facilitating the proximity of $[Fe(CN)_6]^{3-/4-}$ probe.

The effect of periodical light-on-off on MVL ATRP catalyzed by FITC-IgG was investigated by DPV in PBS (pH 7.0) containing 5 mM $[Fe(CN)_6]^{3-/4-}$ and 0.1 M KCl. Polymers/AuNCs/NiNCs/Au electrode prepared at different time was used as a working electrode. As displayed in Fig. 4, DPV peak current was declining when the light was switched on (0–1, 2–3, 4–5, 6–7 h), which indicated the formation of polymers on the

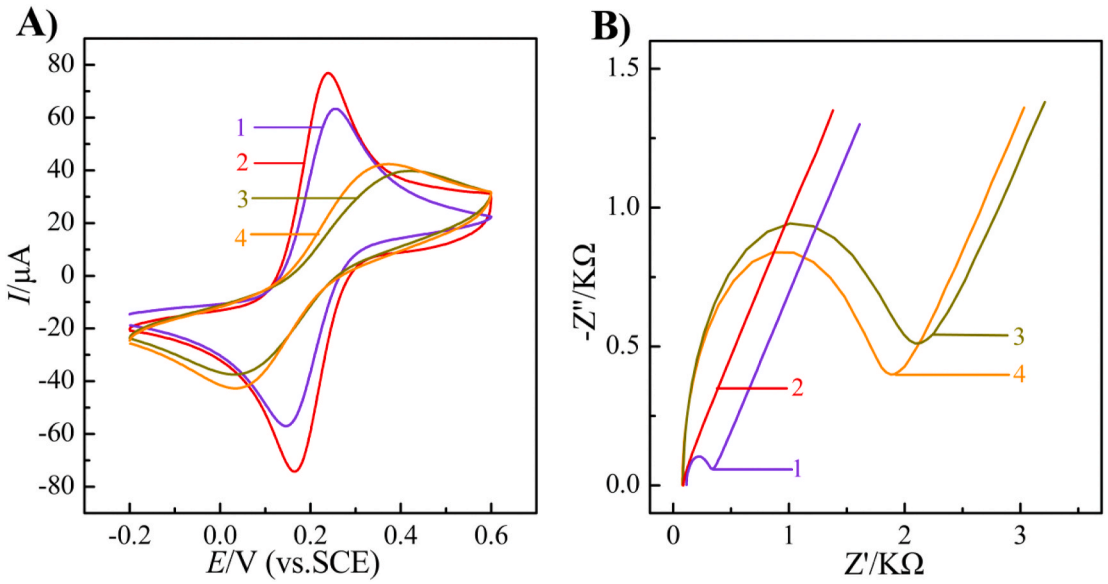

Fig. 3. (A) CVs and (B) EIS recorded on stepwise modified electrodes in PBS (pH 7.0) containing 5 mM $[Fe(CN)_6]^{3-/4-}$ and 0.1 M KCl. The scan rate of CV was 0.1 V/s. The frequency range of EIS was from 5 mHz to 10 kHz (1-bare Au; 2- AuNCs/NiNCs/Au; 3- polymers/AuNCs/NiNCs/Au; 4- IgGIPs/AuNCs/NiNCs/Au).

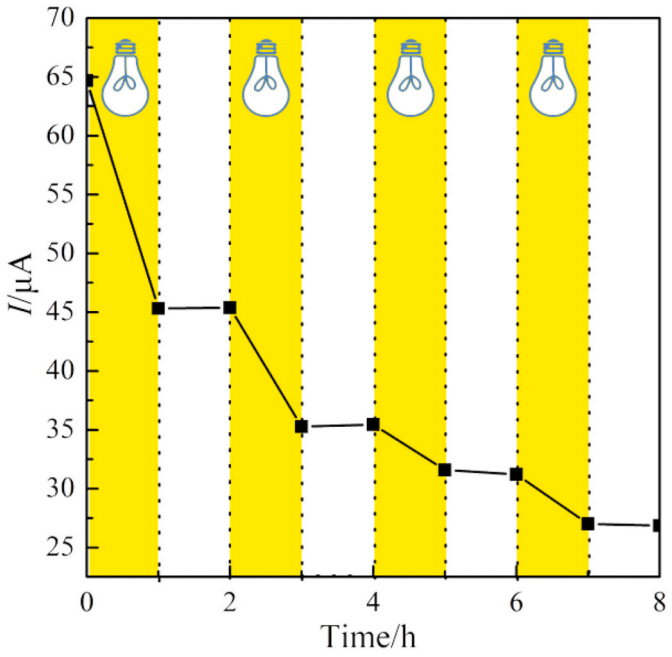

Fig. 4. The "on-off" experiment. (Yellow regions were the visible light "on" and white regions were the visible light "off"). (For interpretation of the references to color in this figure legend, the reader is referred to the Web version of this article.)

surface of electrode. Peak current almost kept unchanged during the dark periods (1–2, 3–4, 5–6, 7–8 h), which may be because there was no inducement of visible light and the polymerization stopped. Multiple controlled "on–off" light switching cycles implied that visible light played a key role to induce ATRP catalyzed by FITC-IgG.

The surface chemical composition of polymers was determined by XPS, and the results were illustrated in Fig. 5. Polymers/AuNCs/NiNCs/Au exhibited O 1s, N 1s, C 1s, Au 4f and Br 3d signals (Fig. 5A), which binding energy were showed at 531.3 eV, 399.6 eV, 285.3 eV, 84.2 eV and 70.1 eV, respectively [41,42]. The Br 3d signal confirmed the successful implementation of MVL ATRP [41]. The inset in Fig. 5A was the fine XPS of S 2p at 161.3 eV. Since S element was from FITC, indicating the successful polymerization catalyzed by FITC-IgG. Fig. 5B was the XPS spectrum of IgGIPs/AuNCs/NiNCs/Au. The peaks of O 1s, N 1s, C 1s, Au 4f and Br 3d showed the binding energy at the similar position with polymers/AuNCs/NiNCs/Au. Compared with Fig. 5A, the disappearance of S 2p binding energy proved the complete removal of FITC from IgGIPs, and would avoid all the effect of FITC on the IgGIPs/AuNCs/NiNCs/Au sensor.

3.2. Optimization of polymerization conditions

The typical conditions such as the ratio of monomer to cross-linker, illumination time, which were important parameters in the experiment and affected the sensing performance of IgGIPs/AuNCs/NiNCs/Au biosensor, were investigated by electrochemical method.

To find the better performance, five IgGIPs/AuNCs/NiNCs/Au electrodes with different ratios of AM to MBA (0.8:1, 1.6:1, 3.2:1, 6.4:1, 12.8:1) were prepared to detect serial concentration of mouse IgG. The sensitivity results of the electrodes were shown in Fig. 6 A. It was seen that lower sensitivity was obtained when the mole ratio was lower than 3.2:1, which could be attributed that the number of AM was too little to form enough binding sites for the protein to enter imprinted holes [43]. When the ratio of AM to MBA was higher than 3.2:1, sensitivity of IgGIPs/AuNCs/NiNCs/Au dropped dramatically, it may be because decreasing cross-linking increased the spatial fluctuations in the recognition sites and hence reduced binding efficiency [44]. Therefore, the ratio of 3.2:1 was chosen as the optimal mole ratio of AM to MBA in the experiment.

The influence of illumination time on IgGIPs/AuNCs/NiNCs/Au was evaluated by CV. As showed in Fig. 6 B, anodic peak current of IgGIPs/AuNCs/NiNCs/Au dropped sharply with the illumination time increasing from 1 to 5 h. When illumination time was higher than 5 h, there was small change in CV peak current. Therefore, illumination time of 5 h was used in subsequent experiments.

3.3. Responses of the IgGIPs/AuNCs/NiNCs/Au toward IgG

IgGIPs/AuNCs/NiNCs/Au could be used as an electrochemical biosensor to detect mouse IgG by DPV. Under the optimized conditions, IgGIPs/AuNCs/NiNCs/Au was prepared and incubated in various concentrations of freshly prepared IgG solution for 5 min. The experimental

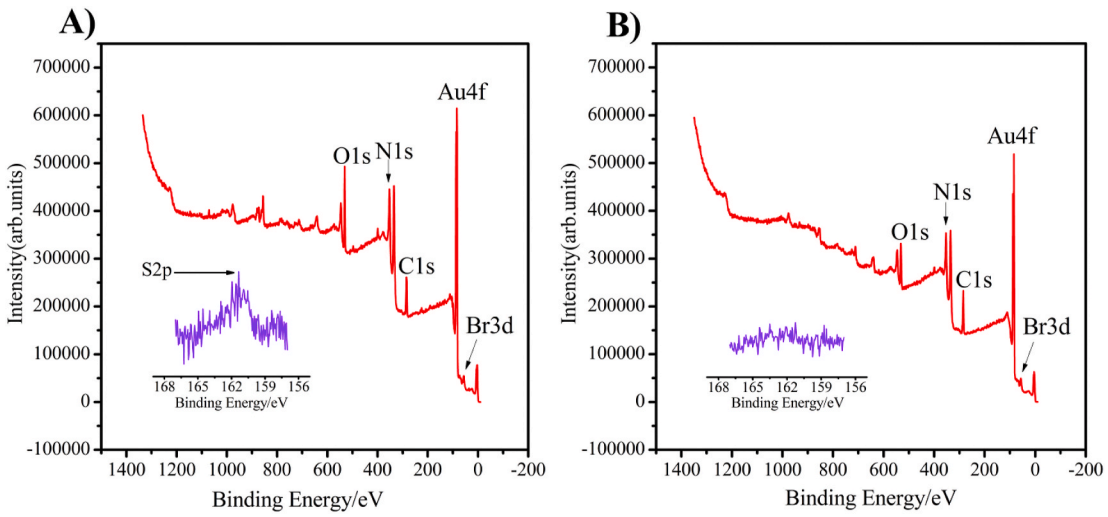

Fig. 5. The XPS spectra of polymers/AuNCs/NiNCs/Au (A) and IgGIPs/AuNCs/NiNCs/Au (B).

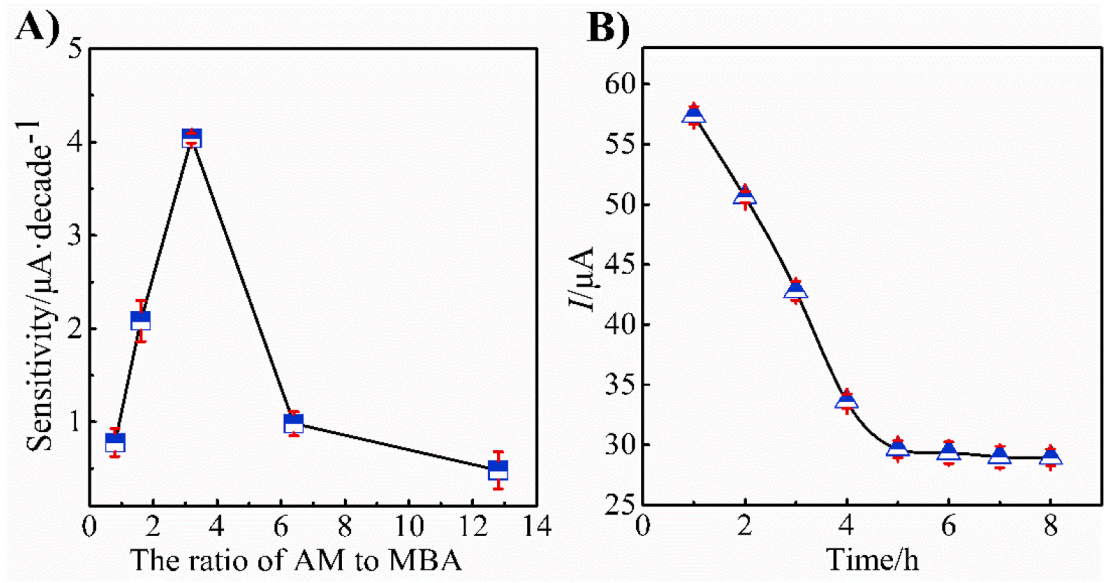

Fig. 6. Effect of the ratio of AM to MBA (A) and the illumination time (B) on IgGIPs/AuNCs/NiNCs/Au.

results were displayed in Fig. 7. It was easy to see that the DPV peak current decreased with the increasing concentration of IgG (Fig. 7A), which may be because that proteins rebound the recognition sites via their complementary spatial structure and appropriate size, thus blocked the $[Fe(CN)_6]^{3-/4-}$ probe from reaching the electrode surface [45,46]. The calibration curve in Fig. 7B showed a good linear relationship between the signal response (ΔI) and logarithm of the IgG concentrations in the range of 1.0×10^{-6} mg L^{-1} to 1.0×10^{1} mg L^{-1}. From the figure, the linear relationship equation was ΔI (μA) = 4.0 logC (mg·L^{-1}) + 36.5 (R^2 = 0.997), and the detection limit (LOD) of 2.0×10^{-8} mg L^{-1} could be estimated (S/N = 3).

When the performance of IgGIPs/AuNCs/NiNCs/Au electrode was compared with sensors for mouse IgG detection including surface plasmon resonance (SPR), electrochemical ELISA, surface-enhanced Raman spectroscopy (SERS) immunoassay and other electrochemical method (as shown in Table 1). It could be seen that the prepared biosensor had lower detection limit and larger linear range.

3.4. Selectivity, repeatability and reproducibility of IgGIPs/AuNCs/NiNCs/Au

Selectivity of IgGIPs/AuNCs/NiNCs/Au toward IgG was investigated by using different protein as interferents by DPV. Fig. 8 showed the signal response (ΔI) of IgGIPs/AuNCs/NiNCs/Au to the same concentration (10^{-4} mg L^{-1}) of IgG, HSA, Hb, Mb, IgM and IgA. Among these, the electrode showed the highest signal response (29.3 ± 0.7 μA) for IgG compared to HSA (1.4 ± 0.3 μA), Hb (2.1 ± 1.2 μA), Mb (1.7 ± 1.2 μA), IgM (1.3 ± 0.3 μA) and IgA (1.3 ± 0.3 μA), which indicated that the shape and size of IgG matched the imprinted "holes"of IgGIPs [51]. In contrast, the signal response (ΔI) of the NIPs were relatively low because there were no imprinted sites in them.

Also, the imprinted polymer efficiency (IE = ΔI_{IgGIPs} / ΔI_{NIPs}) was used to further evaluate the selectivity [52], where ΔI_{IgGIPs} and ΔI_{NIPs} were the signal response of IgGIPs/AuNCs/NiNCs/Au and NIPs/AuNCs/NiNCs/Au, respectively. From Fig. 8, the IE values of IgG, HSA, Hb, Mb, IgM, IgA were 11.9, 1.2, 1.1, 1.4, 1.2 and 1.2, respectively. The largest IE suggested the satisfactory selectivity of IgGIPs/AuNCs/NiNCs/Au towards IgG.

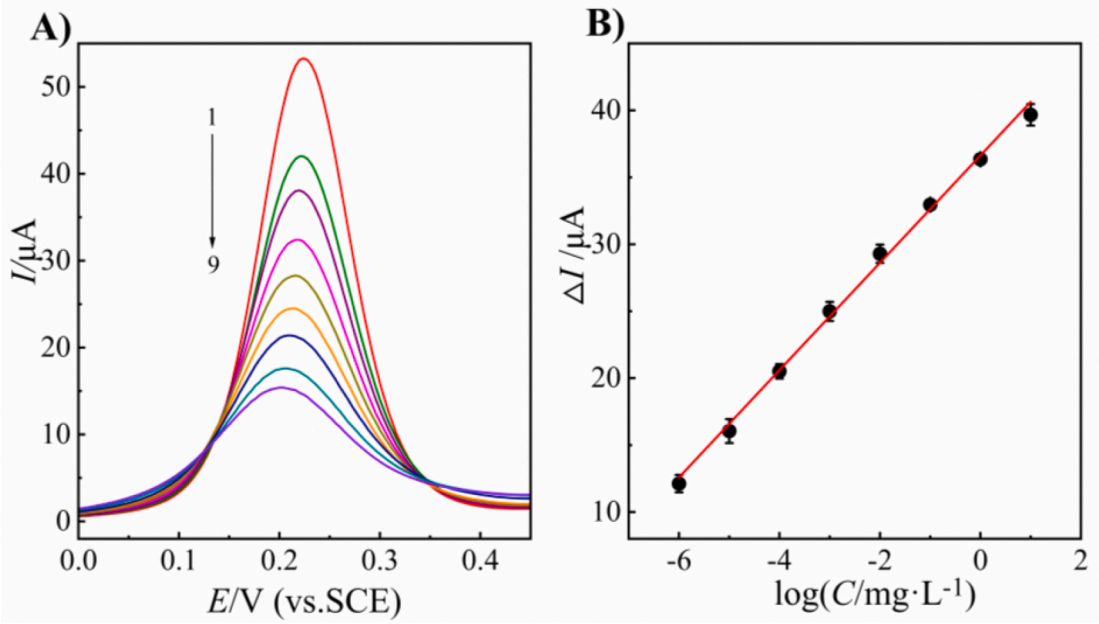

Fig. 7. (A) The DPV curves of IIPs/AuNCs/NiNCs/Au in PBS (pH 7.0) containing 5 mM $[Fe(CN)_6]^{3-/4-}$ + 0.1 M KCl after rebinding with mouse IgG (concentration of mouse IgG from curve 1 to 9 were 0, 1.0×10^{-6}, 1.0×10^{-5}, 1.0×10^{-4}, 1.0×10^{-3}, 1.0×10^{-2}, 1.0×10^{-1}, 1, 10 mg L^{-1}). (B) The calibration plot of IgGIPs/AuNCs/NiNCs/Au.

Table 1
Comparison of some performance of the IgGIPs/AuNCs/NiNCs/Au and reported works for the determination of mouse IgG.

Materials	Method	Linear range (mg·L^{-1})	Detection limit (mg·L^{-1})	Refs.
SPR biosensor based on AgNCs/ chitosan composite	Surface plasmon resonance (SPR)	6.0×10^{-1}–4.0×10^{1}	6.0×10^{-1}	[47]
Two iridium oxide electrodes patterned on a glass substrate	Electrochemical ELISA	5.0×10^{-4}–5.0×10^{-3}	2.0×10^{-4}	[48]
Antigen-assembled gold nanoparticles	Surface-enhanced Raman spectroscopy (SERS) immunoassay	5.0×10^{-5}–5.0×10^{-3}	1.9×10^{-4}	[49]
HRP-based electrochemical immunosensors	Linear sweep voltammetry	1.0×10^{-4}–1.0×10^{-2}	1.0×10^{-4}	[50]
IgGIPs/AuNCs/ NiNCs/Au	DPV	1.0×10^{-6}–1.0×10^{1}	2.0×10^{-8}	This work

The repeatability of the imprinted biosensor was conducted by measuring the DPV response of 10^{-4} mg L^{-1} IgG solution for 3 times using a single electrode. The relative standard deviation (RSD) of 3.6% for IgG concentration was observed, which showed that IgGIPs/AuNCs/NiNCs/Au had good repeatability. To investigate the reproducibility of IgGIPs/AuNCs/NiNCs/Au, three biosensors were fabricated with the same procedure to determine 10^{-4} mg L^{-1} IgG solution. The RSD for determination of IgG concentration was 2.3%, suggesting that the IgGIPs/AuNCs/NiNCs/Au electrode had good reproducibility.

3.5. Application in real samples

Real samples analysis was carried out using standard addition method according to the literatures [3,53]. The purchased mouse IgG sample (serum) was diluted to 1.0×10^{-4} mg L^{-1} and spiked diluted

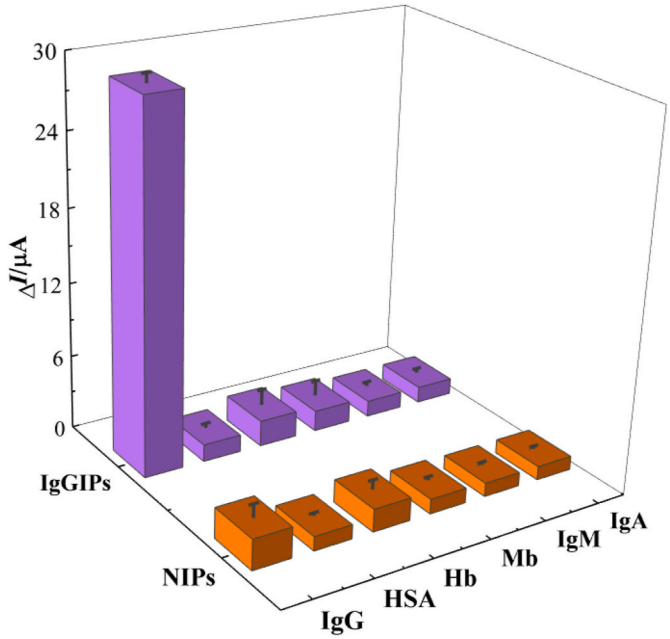

Fig. 8. Signal responses of IgGIPs/AuNCs/NiNCs/Au (IgGIPs) and NIPs/AuNCs/NiNCs/Au (NIPs) for the template (IgG) and interferents (HSA, Hb, Mb, IgM, IgA).

Table 2
Determination of mouse IgG in Real Samples (n = 3).

Analyte	Content (mg·L^{-1})	Added (mg·L^{-1})	Found (mg·L^{-1})	Recovery (%)	RSD (%)
mouse IgG	1.0×10^{-4}	1.0×10^{-4}	2.0×10^{-4}	99.8	3.8
		2.0×10^{-4}	3.0×10^{-4}	102.5	4.1
		5.0×10^{-4}	6.2×10^{-4}	104.8	2.6

with different concentrations of IgG solution of 1.0×10^{-4}, 2.0×10^{-4} and 5.0×10^{-4} mg L^{-1}. The obtained recovery was 99.8, 102.5 and 104.8%, respectively. The results in Table 2 indicated that IgGIPs/AuNCs/NiNCs/Au could be used for quantitative detection of mouse IgG in real samples.

4. Conclusion

This work described a novel electrochemical imprinted biosensor (IgGIPs/AuNCs/NiNCs/Au) for highly selective and sensitive detection of mouse IgG. The imprinted polymers (IgGIPs) were successfully prepared via MVL ATRP with FITC-IgG as both a template and a photocatalyst. After the templates were removed, the photocatalysts (FITC) would not remain in the polymer and avoided all the effect of them on the biosensor. The biosensor was firstly examined by CV, EIS, SEM and XPS. Then the ratio of monomer to cross-linker and illumination time were selected to optimally fabricate the IgGIPs. Finally, the biosensor was successfully applied for the determination of mouse IgG by DPV measurement. The linear range was from 1.0×10^{-6} mg L^{-1} to 1.0×10^{1} mg L^{-1} with a detection limit of 2.0×10^{-8} mg L^{-1} ($S/N = 3$). The results of experiments showed that the proposed biosensor displayed a broader linear range and a lower detection limit for IgG determination when it was compared to those similar sensors.

Credit statement

Ru Bai : Data curation, Writing- Original draft preparation; Yue Sun : Conceptualization , Methodology; Mengyuan Zhao : Data curation, Writing- Original draft preparation; Zhen Han : Formal analysis , Writing- Reviewing and Editing; Juntong Zhang : Formal analysis , Writing- Reviewing and Editing; Yuze Sun : Validation , Writing- Reviewing and Editing; Wenjing Dong : Validation , Writing- Reviewing and Editing; Siyu Li : Validation , Writing- Reviewing and Editing.

Declaration of competing interest

The authors declare that they have no known competing financial interests or personal relationships that could have appeared to influence the work reported in this paper.

Acknowledgements

Authors gratefully acknowledge the financial support from the Science Research Project of Education Department of Liaoning Province (No. LQ2019022), Liaoning BaiQianWan Talents Program (No. 2020921109), High-end Research Incubation Scheme of Liaoning Normal University (GD20L001), the National Natural Science Foundation of China (No. 21304041) and the Innovative Training Program of College Students in Liaoning Normal University (No. 201910165215,202010165158).

References

[1] A.C. Russell, M. Simurina, M.T. Garcia, M. Novokmet, Y. Wang, I. Rudan, H. Campbell, G. Lauc, M.G. Thomas, W. Wang, The N-glycosylation of immunoglobulin G as a novel biomarker of Parkinson's disease, Glycobiology 27 (2017) 501–510.
[2] R. Ma, X. Sun, W. Ha, J. Chen, Y. Shi, Improved surface imprinting based on simplified mass transfer process for the selective extraction of IgG, J. Mater. Chem. B 5 (2017) 7512–7518.
[3] Y. Yang, Q. Liu, Y. Liu, Z. Li, Y. Li, P. Wang, D. Zhang, Z. Zhao, Y. Liu, Y. Dong, An ultrasensitive sandwich-type electrochemical immunosensor based on functionalized mesoporous carbon for IgG detection, RSC Adv. 6 (2016) 31824–31830.
[4] Y. Maki, R. Okamoto, M. Izumi, T. Murase, Y. Kajihara, Semisynthesis of intact complex-type triantennary oligosaccharides from a biantennary oligosaccharide isolated from a natural source by selective chemical and enzymatic glycosylation, J. Am. Chem. Soc. 138 (2016) 3461–3468.
[5] P.F. Jensen, G. Comamala, M.B. Trelle, J.B. Madsen, T.J. Jorgensen, K.D. Rand, Removal of N-linked glycosylations at acidic pH by PNGase A facilitates hydrogen/deuterium exchange mass spectrometry analysis of N-linked glycoproteins, Anal. Chem. 88 (2016) 12479–12488.
[6] U. Kuzmanov, H. Kosanam, E. Diamandis, The sweet and sour of serological glycoprotein tumor biomarker quantification, BMC Med. 11 (2013) 31.
[7] Y. Saylan, R. Uzek, L. Uzun, A. Denizli, Surface imprinting approach for preparing specific adsorbent for IgG separation, J. Biomater. Sci. Polym. Ed. 25 (2014) 881–894.
[8] A. Denizli, Purification of antibodies by affinity chromatography, J. Biol. Chem. 39 (2011) 1–18.
[9] A.A. Shukla, J. Thommes, Recent advances in large-scale production of monoclonal antibodies and related proteins, Trends Biotechnol. 28 (2010) 253–261.
[10] S.R. Stowell, J. Guarner, Role of Serology in the Coronavirus Disease 2019 Pandemic, Clinical Infectious Diseases, 2020 in press.
[11] V.A. Arankalle, K.S. Lole, T.M. Deshmukh, L.P. Chobe, S.S. Gandhe, Evaluation of human (genotype 1) and swine (genotype 4)-ORF2-based ELISAs for anti-HEV IgM and IgG detection in an endemic country and search for type 4 human HEV infections, J. Viral Hepat. 14 (2007) 435–445.
[12] D. Birk, M. Nurminskaya, E. Zycband, Collagen fibrillogenesis in situ: fibril segments undergo post-depositional modifications resulting in linear and lateral growth during matrix development, Developmental Dynamins 202 (1995) 229–243.
[13] T. Tanaka, T. Matsunaga, Fully automated chemiluminescence immunoassay of insulin using antibody-protein A-bacterial magnetic particle complexes, Anal. Chem. 72 (2000) 3518–3522.
[14] A. Tavares, M. Sales, Novel electro-polymerized protein-imprinted materials using Eriochrome black T: application to BSA sensing, Electrochim. Acta 262 (2018) 214–225.
[15] R. Horikawa, H. Sunayama, Y. Kitayama, E. Takano, T. Takeuchi, A programmable signaling molecular recognition nanocavity prepared by molecular imprinting and post-imprinting modifications, Angew. Chem. 55 (2016) 13023–13027.
[16] A. Kawamura, T. Kiguchi, T. Nishihata, T. Uragami, T. Miyata, Target molecule-responsive hydrogels designed via molecular imprinting using bisphenol A as a template, Chem. Commun. 50 (2014) 11101–11103.
[17] Z. Zhang, Y. Guan, M. Li, A. Zhao, J. Ren, X. Qu, Highly stable and reusable imprinted artificial antibody used for in situ detection and disinfection of pathogens, Chem. Sci. 6 (2015) 2822–2826.
[18] E. Verheyen, J.P. Schillemans, M. van Wijk, M.A. Demeniex, W.E. Hennink, C. F. van Nostrum, Challenges for the effective molecular imprinting of proteins, Biomaterials 32 (2011) 3008–3020.
[19] K. Flavin, M. Resmini, Imprinted nanomaterials: a new class of synthetic receptors, Anal. Bioanal. Chem. 393 (2009) 437–444.
[20] Y.P. Huang, Z.S. Liu, C.R.Y. Zheng, Gao, Recent developments of molecularly imprinted polymer in CEC, Electrophoresis 30 (2009) 155–162.
[21] S. Nishitani, T. Sakata, Potentiometric adsorption isotherm analysis of a molecularly imprinted polymer interface for small-biomolecule recognition, ACS Omega 3 (2018) 5382–5389.
[22] H. Guo, D. Yuan, G. Fu, Enhanced surface imprinting of lysozyme over a new kind of magnetic chitosan submicrospheres, J. Colloid Interface Sci. 440 (2015) 53–59.
[23] K. Matyjaszewski, Dvanced materials by atom transfer radical polymerization, Adv. Mater. 30 (2018) 1706441.
[24] M. Chen, H. Gong, Y. Gu, Controlled/living radical polymerization of semifluorinated (meth) acrylates, Synlett 29 (2018) 1543–1551.
[25] Y. Sun, X. Feng, J. Hu, S. Bo, J. Zhang, W. Wang, S. Li, Y. Yang, Preparation of hemoglobin (Hb)-imprinted poly(ionic liquid)s via Hb-catalyzed eATRP on gold nanodendrites, Anal. Bioanal. Chem. 412 (2020) 983–991.
[26] E. Yildirim, E. Turan, T. Caykara, Construction of myoglobin imprinted polymer films by grafting from silicon surface, J. Mater. Chem. 22 (2012) 636–642.
[27] R. Naraprawatphong, G. Kawanaka, M. Hayashi, A. Kawamura, T. Miyata, Development of protein-recognition SPR devices by combination of SI-ATRP with biomolecular imprinting using protein ligands, Molecular Imprinting 4 (2016) 21–30.
[28] Q.Q. Gai, F. Qu, T. Zhang, Y.K. Zhang, The preparation of bovine serum albumin surface-imprinted superparamagnetic polymer with the assistance of basic functional monomer and its application for protein separation, J. Chromatogr. A 1218 (2011) 3489–3495.
[29] D. Wei, Y. Xu, C. Liu, Y. Zhai, H. Chen, L. Bai, H. Yang, L. Yang, W. Wang, Y. Niu, Visible light-induced metal-free atom transfer radical polymerization: an efficient approach to polyacrylonitrile, J. Polym. Sci. Polym. Chem. 57 (2019) 1265–1269.
[30] C. Aydogan, C. Kutahya, A. Allushi, G. Yilmaz, Y. Yagci, Block copolymer synthesis in one shot: concurrent metal-free ATRP and ROP processes under sunlight, Polym. Chem. 8 (2017) 2899–2903.
[31] X. Pan, C. Fang, M. Fantin, N. Malhotra, W.Y. So, L.A. Peteanu, A.A. Isse, A. Gennaro, P. Liu, K. Matyjaszewski, Mechanism of photoinduced metal-free atom transfer radical polymerization: experimental and computational studies, J. Am. Chem. Soc. 138 (2016) 2411–2425.
[32] K. Pan, R. Ren, H. Li, B. Cao, Preparation of dual stimuli-responsive PET track-etched membrane by grafting copolymer using ATRP, Polym. Adv. Technol. 24 (2013) 22–27.
[33] Z. Guan, B. Smart, A remarkable visible light effect on atom-transfer radical polymerization, Macromolecules 33 (2000) 6904–6906.
[34] X. Liu, L. Zhang, Z. Cheng, X. Zhu, Metal-free photoinduced electron transfer - atom transfer radical polymerization (PET-ATRP) via a visible light organic photocatalyst, Polym. Chem. 7 (2016) 689–700.
[35] M. Neumann, S. Fuldner, B. Konig, K. Zeitler, Metal-free, cooperative asymmetric organophotoredox catalysis with visible light, Angew. Chem. 50 (2011) 951–954.

[36] Y. Sun, M. Zhao, Y. Liu, L. Fu, S. Li, Y. Yang, Preparation of erythromycin imprinted polymer by metal-free visible-light–induced ATRP and its application in sensor, J. Solid State Electrochem. 23 (2018) 583–590.
[37] Y. Sun, H. Du, Y. Deng, Y. Lan, C. Feng, Preparation of polyacrylamide via surface-initiated electrochemical-mediated atom transfer radical polymerization (SI-eATRP) for Pb^{2+} sensing, J. Solid State Electrochem. 20 (2015) 105–113.
[38] Y. Sun, H. Du, Y. Lan, W. Wang, Y. Liang, C. Feng, M. Yang, Preparation of hemoglobin (Hb) imprinted polymer by Hb catalyzed eATRP and its application in biosensor, Biosens. Bioelectron. 77 (2016) 894–900.
[39] S. Yue, Y. Lan, L. Yang, F. Kong, H. Du, C. Feng, Preparation of hemoglobin imprinted polymers based on graphene and protein removal assisted by electric potential, RSC Adv. 6 (2016) 61897–61905.
[40] K. Ghanbari, M. Roushani, A nanohybrid probe based on double recognition of an aptamer MIP grafted onto a MWCNTs-Chit nanocomposite for sensing hepatitis C virus core antigen, Sensor. Actuator. B Chem. 258 (2018) 1066–1071.
[41] Y. Yang, X. Liu, G. Ye, S. Zhu, Z. Wang, X. Huo, K. Matyjaszewski, Y. Lu, J. Chen, Metal-free photoinduced electron transfer-atom transfer radical polymerization integrated with bioinspired polydopamine chemistry as a green strategy for surface engineering of magnetic nanoparticles, ACS Appl. Mater. Interfaces 9 (2017) 13637–13646.
[42] G. Maduraiveeran, R. Rasik, M. Sasidharan, W. Jin, Bimetallic gold-nickel nanoparticles as a sensitive amperometric sensing platform for acetaminophen in human serum, J. Electroanal. Chem. 808 (2018) 259–265.
[43] W. Lian, S. Liu, J. Yu, X. Xing, J. Li, M. Cui, J. Huang, Electrochemical sensor based on gold nanoparticles fabricated molecularly imprinted polymer film at chitosan-platinum nanoparticles/graphene-gold nanoparticles double nanocomposites modified electrode for detection of erythromycin, Biosens. Bioelectron. 38 (2012) 163–169.
[44] M. Zayats, M. Kanwar, M. Ostermeier, P.C. Searson, Molecular imprinting of maltose binding protein: tuning protein recognition at the molecular level, Macromolecules 44 (2011) 3966–3972.
[45] S. Motia, B. Bouchikhi, N. El Bari, An electrochemical molecularly imprinted sensor based on chitosan capped with gold nanoparticles and its application for highly sensitive butylated hydroxyanisole analysis in foodstuff products, Talanta 223 (2021) 121689.
[46] Y. Sun, S. Li, Y. Yang, X. Feng, W. Wang, Y. Liu, M. Zhao, Z. Zhang, Fabrication of a thermal responsive hemoglobin (Hb) biosensor via Hb-catalyzed eATRP on the surface of ZnO nanoflowers, J. Electroanal. Chem. 848 (2019) 113346.
[47] D. Zhang, Y. Sun, Q. Wu, P. Ma, H. Zhang, Y. Wang, D. Song, Enhancing sensitivity of surface plasmon resonance biosensor by Ag nanocubes/chitosan composite for the detection of mouse IgG, Talanta 146 (2016) 364–368.
[48] M. Wilson, Electrochemical immunosensors for the simultaneous detection of two tumor markers, Anal. Chem. 77 (2005) 1496–1502.
[49] A. Lopez, F. Lovato, S.H. Oh, Y.H. Lai, S. Filbrun, E.A. Driskell, J.D. Driskell, SERS immunoassay based on the capture and concentration of antigen-assembled gold nanoparticles, Talanta 146 (2016) 388–393.
[50] H.J. Kang, M.â.A. Aziz, B. Jeon, K. Jo, H. Yang, Strategy for low background-current levels in the electrochemical biosensors using horse-radish peroxidase labels, Electroanalysis 21 (2009) 2647–2652.
[51] Y. Sun, J. Zhang, J. Li, M. Zhao, Y. Liu, Preparation of protein imprinted polymers via protein-catalyzed eATRP on 3D gold nanodendrites and their application in biosensors, RSC Adv. 7 (2017) 28461–28468.
[52] N. Casis, C. Busatto, M.M. Fidalgo de Cortalezzi, S. Ravaine, D.A. Estenoz, Molecularly imprinted hydrogels from colloidal crystals for the detection of progesterone, Polym. Int. 64 (2015) 773–779.
[53] Q. Zhao, Q. Wu, P. Ma, L. Xu, F. Zhang, D. Li, X. Liu, S. Xu, Y. Sun, D. Song, X. Wang, Selective and sensitive fluorescence detection method for pig IgG based on competitive immunosensing strategy and magnetic bioseparation, Talanta 195 (2019) 103–108.